Gluon parton distribution of the nucleon from (2 + 1 + 1)-flavor lattice QCD in the physical-continuum limit

Zhouyou Fan,[1] William Good,[1,2] and Huey-Wen Lin[1,2]

[1]*Department of Physics and Astronomy, Michigan State University, East Lansing, Michigan 48824, USA*
[2]*Department of Computational Mathematics, Science and Engineering, Michigan State University, East Lansing, Michigan 48824, USA*

We present the first physical-continuum limit x-dependent nucleon gluon distribution from lattice QCD using the pseudo-PDF approach, on lattice ensembles with $2 + 1 + 1$ flavors of highly improved staggered quarks (HISQ), generated by MILC Collaboration. We use clover fermions for the valence action on three lattice spacings $a \approx 0.9$, 0.12 and 0.15 fm and three pion masses $M_\pi \approx 220$, 310 and 690 MeV, with nucleon two-point measurements numbering up to $O(10^6)$ and nucleon boost momenta up to 3 GeV. We study the lattice-spacing and pion-mass dependence of the reduced pseudo–Ioffe-time distribution matrix elements obtained from the lattice calculation, then extrapolate them to the continuum-physical limit before extracting $xg(x)/\langle x \rangle_g$. We use the gluon momentum fraction $\langle x \rangle_g$ calculated from the same ensembles to determine the nucleon gluon unpolarized PDF $xg(x)$ for the first time entirely through lattice-QCD simulation. We compare our results with previous single-ensemble lattice calculations, as well as selected global fits.

I. INTRODUCTION

Many precision phenomenology and theoretical predictions for hadron colliders rely on accurate estimates of the uncertainty in Standard-Model (SM) predictions. Among these predictions, the parton distribution functions (PDFs), the nonperturbative functions quantifying probabilities for finding quarks and gluons in hadrons with particular momentum fraction, are particularly important inputs in high-energy scattering [1–11]. The gluon PDF $g(x)$ needs to be known precisely to calculate the cross section for these processes in pp collisions, such as the cross section for Higgs-boson production and jet production at the Large Hadron Collider (LHC) [12,13], and direct J/ψ photo-production at Jefferson Lab [14]. The future U.S.-based Electron-Ion Collider (EIC) [15], planned to be built at Brookhaven National Lab, will further our knowledge of the gluon PDF [16–18]. In Asia, the Electron-Ion Collider in China (EicC) [19] is also planned to impact our understanding of the gluon and sea-quark distributions. Although significant efforts to extract the gluon distribution $g(x)$ have been made in the last decade, there are still problems in obtaining a precise $g(x)$ in the large-x region.

Lattice quantum chromodynamics (QCD) is a nonperturbative theoretical method for calculating QCD quantities that has full systematic control. Calculations of x-dependent hadron structure in lattice QCD have multiplied since the proposal of large-momentum effective theory (LaMET) [20–22]. Many lattice works have been done on nucleon and meson PDFs, and generalized parton distributions (GPDs) based on the quasi-PDF approach [23–55]. Alternative approaches to lightcone PDFs in lattice QCD are the Compton-amplitude approach (or "OPE without OPE") [56–68], the "hadronic-tensor approach" [69–74], the "current-current correlator" [48,63,75–80] and the pseudo-PDF approach [78,81–97]. A few works have started to include lattice-QCD systematics, such as finite-volume effects, in their calculations [39,80]. However, most these calculations are still, at the current stage, done with a single lattice spacing. Most lattice calculations of PDFs use next-to-leading-order (NLO) matching or, equivalently, NLO Wilson coefficients [22,98–100], and some lattice calculations of the valence pion PDF [101] have incorporated NNLO matching [46,102]. More work is needed to reduce high-twist systematics and improve the lattice determination of small-x and antiquark PDFs with very large boost momenta.

Recently, progress has been made in the most-calculated isovector quark distribution of nucleon by MSULat [49], ETMC [51], and HadStruc Collaborations [103], who studied lattice-spacing dependence. MSULat studied three

lattice spacings (0.09, 0.12, and 0.15 fm) and pion masses (135, 220, 310 MeV) and performed a simultaneous continuum-physical extrapolation using a third-order z-expansion on renormalized LaMET matrix elements [49] with nucleon boost momenta around 2.2 and 2.6 GeV. ETMC also uses three lattice spacings, 0.06, 0.08, and 0.09 fm, but with heavier pion mass (370 MeV) and investigated the continuum extrapolation of the data on renormalized LaMET matrix elements with boost momentum around 1.8 GeV [51]. HadStruc Collaboration studied three lattice spacings, 0.048, 0.065, and 0.075 fm with two-flavor 440-MeV lattice ensembles using the continuum pseudo–Ioffe-time distribution (ITD) [103]. Most of the works above found mild nonzero dependence on lattice spacing (varying with the Wilson-link displacement) in the nucleon case for LaMET or pseudo-ITD matrix elements.

In contrast with the quark PDFs, there are fewer gluon-PDF calculations, due to their notoriously noisier matrix elements on the lattice. To date, there have only been a few exploratory gluon-PDF calculations for unpolarized nucleon [36,92,95], pion [96], and kaon [104], and polarized nucleon [97] using the pseudo-PDF [105] and quasi-PDF [38,106] methods. Most of these calculations, like many exploratory lattice calculations, are done only using one lattice spacing at heavy pion mass.

In this work, we report the first continuum-limit unpolarized gluon PDF of nucleon study using three lattice spacings: 0.09, 0.12, and 0.15 fm with pion mass ranging from 220 to 700 MeV using the pseudo-PDF method. The remainder of this paper is organized as follows: In Sec. II, we present the procedure for how the lattice correlators are calculated and analyzed to extract the ground-state matrix elements for the pseudo-PDF method. We then study the lattice-spacing dependence of matrix elements at 310 and 700-MeV pion mass in Sec. III, checking both $O(a)$ and $O(a^2)$ forms using multiple continuum-extrapolation strategies. We perform a physical-continuum extrapolation to obtain continuum reduced pseudo-ITDs (RpITDs) matrix element, before final determination of the nucleon unpolarized gluon PDF $xg(x)$ is obtained from the $xg(x)/\langle x \rangle_g$ and $\langle x \rangle_g$ results. Using the gluon momentum fraction calculated on the same ensemble, we obtain the gluon PDF and compare with the phenomenological global-fit PDF results. We consider the quark-mixing systematics, but they are found to be small. The final conclusion and future outlook can be found in Sec. IV.

II. LATTICE SETUP, CORRELATORS AND MATRIX ELEMENTS

This calculation is carried out using four ensembles with $N_f = 2 + 1 + 1$ highly improved staggered quarks (HISQ) [107], generated by the MILC Collaboration [108], with three different lattice spacings ($a \approx 0.9$, 0.12 and 0.15 fm) and three pion masses (220, 310, 690 MeV); see Table I for more details. We apply five steps of hypercubic

TABLE I. Lattice spacing a, valence pion mass (M_π^{val}) and η_s mass ($M_{\eta_s}^{\mathrm{val}}$), lattice size ($L^3 \times T$), number of configurations (N_{cfg}), number of total two-point correlator measurements ($N_{\mathrm{meas}}^{\mathrm{2pt}}$), and source-sink separation times t_{sep} used in the three-point correlator fits of $N_f = 2 + 1 + 1$ clover valence fermions on HISQ ensembles generated by the MILC Collaboration and analyzed in this study.

Ensemble	a09m310	a12m220	a12m310	a15m310
a (fm)	0.0888(8)	0.1184(10)	0.1207(11)	0.1510(20)
$L^3 \times T$	$32^3 \times 96$	$32^3 \times 64$	$24^3 \times 64$	$16^3 \times 48$
M_π^{val} (GeV)	0.313(1)	0.2266(3)	0.309(1)	0.319(3)
$M_{\eta_s}^{\mathrm{val}}$ (GeV)	0.698(7)	N/A	0.6841(6)	0.687(1)
P_z (GeV)	[0, 3.05]	[0, 2.29]	[0, 2.14]	[0, 2.56]
N_{cfg}	1009	957	1013	900
$N_{\mathrm{meas}}^{\mathrm{2pt}}$	387,456	1,466,944	324,160	259,200
t_{sep}	[6, 10]	[6, 10]	[5, 9]	[4, 8]

(HYP) smearing [109] to the gauge links to reduce short-distance noise. Wilson-clover fermions are used in the valence sector, and the valence-quark masses are tuned to reproduce the lightest light and strange sea pseudoscalar meson masses (which correspond to pion masses 310 and 690 MeV, respectively). A similar setup is used by PNDME collaboration [110–121] with local operators, such as isovector and flavor-diagonal charges, form factors and moments; the results from this mixed-action setup are consistent with the same physical quantities calculated using different fermion actions [55,122–126].

On each lattice configuration, we calculate the nucleon two-point correlators using multiple sources:

$$C_N^{2\mathrm{pt}}(P_z; t) = \langle 0 | \Gamma \int d^3 y\, e^{-iyP_z} \chi(\vec{y}, t) \chi(\vec{0}, 0) | 0 \rangle, \quad (1)$$

with the nucleon interpolation operator χ as $\epsilon^{lmn}[u(y)^{lT} i\gamma_4\gamma_2\gamma_5 d^m(y)] u^n(y)$ (where $\{l, m, n\}$ are color indices, $u(y)$ and $d(y)$ are quark fields), the projection operator $\Gamma = \frac{1}{2}(1 + \gamma_4)$, t is lattice Euclidean time, and P_z is the nucleon boost momentum along the spatial z-direction. We use Gaussian momentum smearing [127] on the quark field to improve the signal for nucleon boost momenta up to 3.0 GeV. Hundreds of thousands of measurements are made, varying for different ensembles. Compared to our previous nucleon gluon PDF calculation on one a12m310 ensemble with 10^5 measurements [92], this study uses more measurements and varies the lattice spacing. We then calculate the three-point gluon correlator by combining the gluon loop with nucleon two-point correlators,

$$C_N^{3\mathrm{pt}}(z, P_z; t_{\mathrm{sep}}, t)$$
$$= \langle 0 | \Gamma \int d^3 y\, e^{-iyP_z} \chi(\vec{y}, t_{\mathrm{sep}}) \mathcal{O}_g(z, t) \chi(\vec{0}, 0) | 0 \rangle, \quad (2)$$

where t is the gluon-operator insertion time, t_{sep} is the source-sink time separation. $\mathcal{O}_g(z,t)$ is the gluon operator introduced in Ref. [105]:

$$\mathcal{O}(z) \equiv \sum_{i \neq z,t} \mathcal{O}(F^{ti}, F^{ti}; z) - \frac{1}{4} \sum_{i,j \neq z,t} \mathcal{O}(F^{ij}, F^{ij}; z), \quad (3)$$

where the operator $\mathcal{O}(F^{\mu\nu}, F^{\alpha\beta}; z) = F^\mu_\nu(z)U(z,0)F^\alpha_\beta(0)$ with $U(z,0)$ being the straight-line gauge link, and z is the Wilson link length. To extract the ground-state matrix element, we use a two-state fit on the two-point correlators and a two-sim fit on the three-point correlators:

$$C_N^{2\text{pt}}(P_z,t) = |A_{N,0}|^2 e^{-E_{N,0}t} + |A_{N,1}|^2 e^{-E_{N,1}t} + \dots, \quad (4)$$

$$\begin{aligned} C_N^{3\text{pt}}(z, P_z, t, t_{\text{sep}}) = &|A_{N,0}|^2 \langle 0|O_g|0\rangle e^{-E_{N,0}t_{\text{sep}}} \\ &+ |A_{N,0}||A_{N,1}|\langle 0|O_g|1\rangle e^{-E_{N,1}(t_{\text{sep}}-t)}e^{-E_{N,0}t} \\ &+ |A_{N,0}||A_{N,1}|\langle 1|O_g|0\rangle e^{-E_{N,0}(t_{\text{sep}}-t)}e^{-E_{N,1}t} \\ &+ |A_{N,1}|^2 \langle 1|O_g|1\rangle e^{-E_{N,1}t_{\text{sep}}} + \dots, \quad (5) \end{aligned}$$

where the $|A_{N,i}|^2$ and $E_{N,i}$ are the ground-state ($i=0$) and first excited state ($i=1$) amplitude and energy, respectively.

To visualize our fitted matrix-element extraction, we compare to ratios of the three-point to the two-point correlator

$$R_N(z, P_z, t_{\text{sep}}, t) = \frac{C_N^{3\text{pt}}(z, P_z, t, t_{\text{sep}})}{C_N^{2\text{pt}}(P_z, t_{\text{sep}})}. \quad (6)$$

The left-hand side of Fig. 1 shows example ratios for the gluon matrix elements from all four ensembles at pion masses $M_\pi \in \{220, 310\}$ MeV at selected momenta P_z and Wilson-line length z. The left column shows the ratio plots with data points of R from different source-sink separation, t_{sep}, along with the reconstructed bands from the fit, showing how well the fit describing the data in Eq. (6); the final ground-state matrix elements are shown in gray bands. We observe that the ratios increase with increasing source-sink separation t_{sep} and continuously approach the ground-state matrix elements obtained from the simultaneous two-state fit to three-point correlators with five inputs of t_{sep}. The middle and right columns of Fig. 1 show how the ground-state matrix elements vary with $t_{\text{sep}}^{\min}$ and $t_{\text{sep}}^{\max}$ with the same $t_{\text{sep}}^{\max}$ and $t_{\text{sep}}^{\min}$ used in the left column, respectively. The gray bands in each plot of the middle and right columns are the same ground-state matrix elements extracted from the fit shown in the corresponding plots in left column; these demonstrate how stable our ground-state matrix element extractions are. We observe that overall the ground-state matrix elements are consistent with each other

within one standard deviation with different $t_{\text{sep}}^{\min}$ choices. There seems to be some hint of $t_{\text{sep}}^{\max}$-dependence in the ground-state matrix elements, but they do converge. Taking the a12m220 ensemble as an example, we observe larger fluctuations in the matrix-element extractions when small $t_{\text{sep}}^{\min} = 3$, or small $t_{\text{sep}}^{\max} = 6$ and 7, are used. The ground-state matrix element extracted from two-sim fits comes into reasonable agreement when $t_{\text{sep}}^{\min} > 5$ and $t_{\text{sep}}^{\max} > 8$. Similar results are observed with the nucleon when calculated at strange-quark mass, as shown in Fig. 2.

III. RESULTS AND DISCUSSIONS

A. Lattice-spacing dependence of RpITDs

Using the nucleon ground-state matrix elements, we can now compute the reduced Ioffe-time pseudodistribution (RpITD) [81,82,106,128]

$$\mathcal{M}(\nu, z^2) = \frac{\mathcal{M}(zP_z, z^2)/\mathcal{M}(0 \cdot P_z, 0)}{\mathcal{M}(z \cdot 0, z^2)/\mathcal{M}(0 \cdot 0, 0)}, \quad (7)$$

where Ioffe time $\nu = zP_z$, and $\mathcal{M}(\nu, z^2)$ are the nucleon matrix elements at boost momentum P_z and gluon operators with Wilson displacement z. By construction, the renormalization of $\mathcal{O}(z)$ and kinematic factors are canceled in the RpITDs, and the ultraviolet divergences are removed. The RpITD double ratios employed here are normalized to one at $z=0$, and the lattice systematics are reduced due to the double ratio. These RpITDs will be input into the pseudo-PDF framework detailed in Ref. [81] to obtain the unpolarized nucleon gluon PDFs.

We first examine the pion-mass and lattice-spacing dependence of the nucleon gluon RpITDs. The top panel of Fig. 3 shows the RpITDs at boost momentum around 1.3 GeV as functions of Ioffe time ν for the a12m220, a09m310, a12m310, and a15m310 ensembles. Note that given the different size of the lattice dimensions and lattice spacings, there is no easy way to use the same boost momentum for all four ensembles. For the a12m310, a12m220, and a09m310 ensembles, we are able to find close momenta, but the boost momentum on a15m310 is not so close, 1.54 GeV. Nevertheless, this allows us to study the lattice-spacing and pion-mass dependence without any interpolation; we find in both cases mild dependence. The $a = 0.12$ fm ensembles seem to prefer slightly higher central values for the RpITDs, but they are consistent with those from a09m310 and a15m310 within one standard deviation.

We then choose a fixed pion mass and Ioffe time ν to explore the lattice-spacing dependence in more detail. We examine the RpITDs at three values of z and set $n_z \in \{4, 3, 2\}$ in lattice units ($P_z = \frac{2\pi}{L}n_z$) for the a09m310, a12m310, and a15m310 ensembles, respectively, to check the lattice-spacing dependence, where the Ioffe time
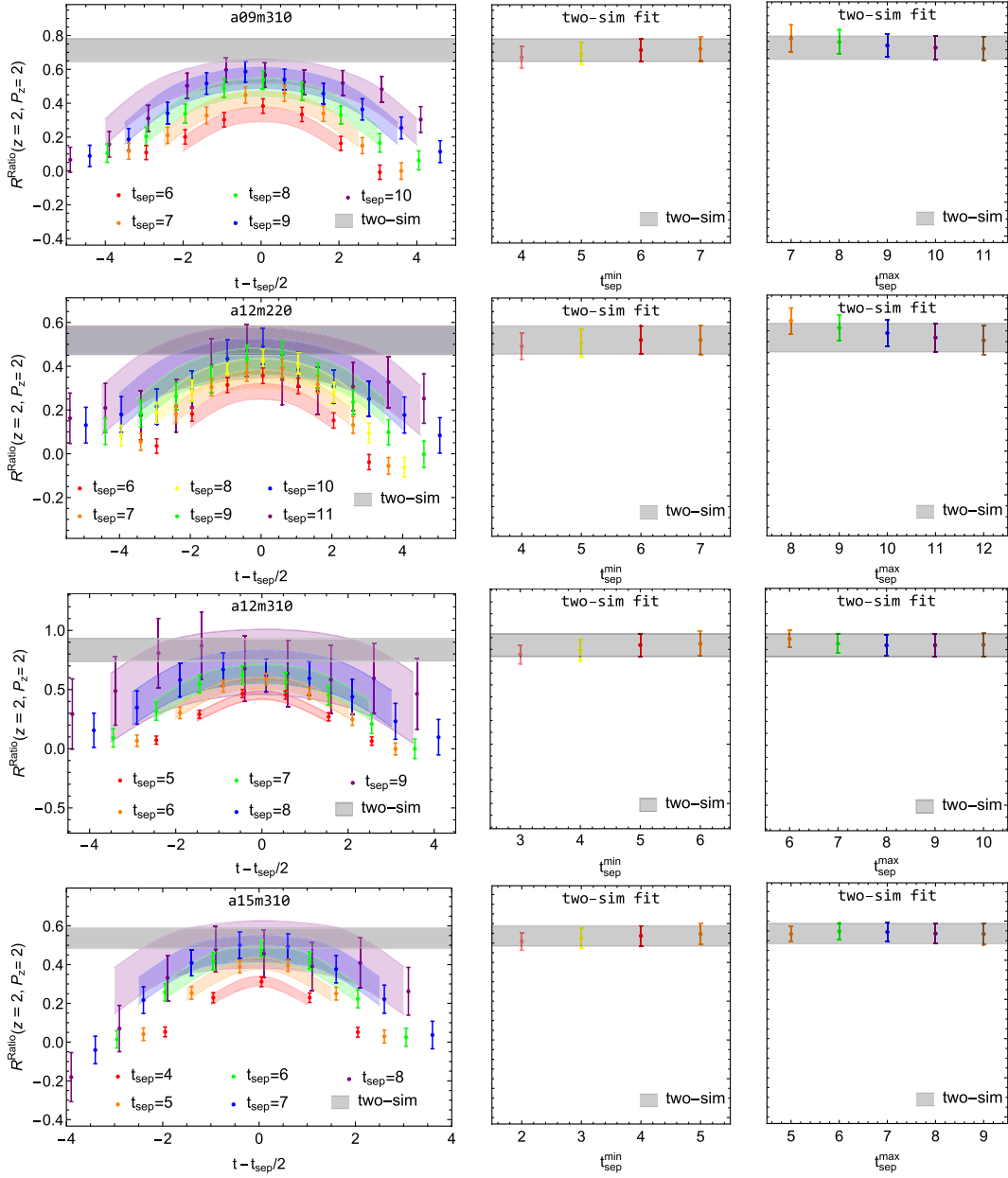
FIG. 1. Example ratio plots (left) and two-sim fits (last 2 columns) of the light nucleon correlators at pion masses $M_\pi \approx \{310, 220, 310, 310\}$ MeV from the a09m310, a12m220, a12m310, and a15m310 ensembles. The gray band shown on each plot is the extracted ground-state matrix element from the two-sim fit that we use as our best value. From left to right, the columns are: the ratio of the three-point to two-point correlators with the reconstructed fit bands from the two-sim fit using the final t_{sep} inputs, shown as functions of $t - t_{\text{sep}}/2$, the two-sim fit results using $t_{\text{sep}} \in [t_{\text{sep}}^{\min}, t_{\text{sep}}^{\max}]$ varying $t_{\text{sep}}^{\min}$ and $t_{\text{sep}}^{\max}$.

$\nu = z P_z$ are the same for all ensembles. We assume a linear $O(a)$ or $O(a^2)$ dependence and fit the RpITD data:

$$\mathcal{M}(\nu, z^2, a, M_\pi) = \mathcal{M}^{\text{cont}} + c_a a^n \tag{8}$$

for $n = 1$ and 2, respectively. The fit results are shown in Fig. 4 for both light and strange nucleons at $\nu = \{\pi/4, \pi/2, \pi\}$. All the plots show the RpITD points

at a fixed ν are consistent within one-sigma error; however, there seems to be a trend that the lattice-spacing dependence is slightly stronger at larger ν, making the continuum-extrapolated results larger. The χ^2/dof are all within one standard deviation of 0.5, showing that there is no preference in choice of ν in this respect. In both $O(a)$ and $O(a^2)$ extrapolation, the light and strange nucleons appear to have opposite trends with lattice spacing; however,
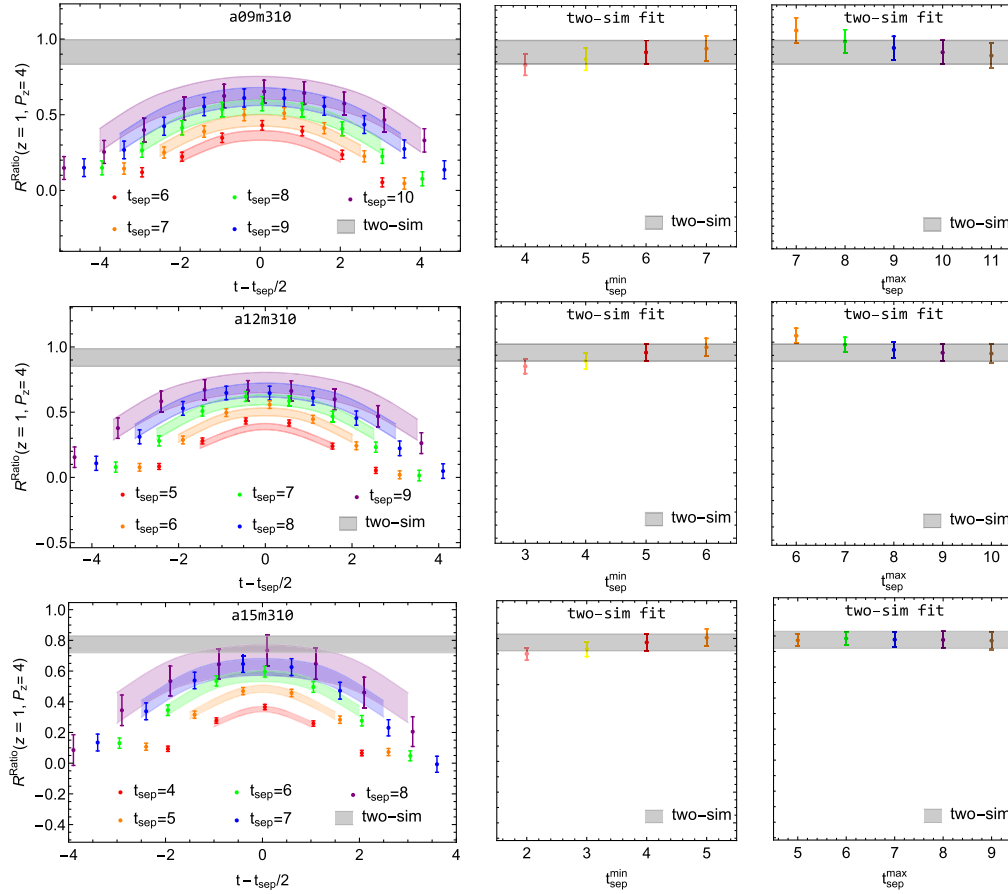
FIG. 2.   Example ratio plots (left), and two-sim fits (last 2 columns) of the strange nucleon correlators at pion mass $M_\pi \approx 700$ MeV from the a09m310, a12m220, a12m310, and a15m310 ensembles. The gray band shown on each plot is the extracted ground-state matrix element from the two-sim fit that we use as our best value. From left to right, the columns are: the ratio of the three-point to two-point correlators with the reconstructed fit bands from the two-sim fit using the final $t_{\rm sep}$ inputs, shown as functions of $t - t_{\rm sep}/2$, the two-sim fit results using $t_{\rm sep} \in [t_{\rm sep}^{\rm min}, t_{\rm sep}^{\rm max}]$ varying $t_{\rm sep}^{\rm min}$ and $t_{\rm sep}^{\rm max}$.

the slopes of the fits are consistent with zero within one standard deviation for each pion mass over all the selected ν. Corresponding to a reading of Fig. 4 left to right, top to bottom, the $O(a)\mathcal{M}^{\rm cont}$ are 0.988(31), 0.95(12), 0.70(32), 0.994(15), 0.978(54), and 0.87(16). The $O(a^2)$ values are 0.987(16), 0.950(60), 0.75(16), 0.9997(80), 0.959(29), and 0.837(84). The deviation of the continuum-limit RpITD increases as ν increases, with the continuum-limit error at $\nu = \pi$ consistently being about a factor of ten larger than those at $\nu = \pi/4$. The continuum-limit RpITDs using a and a^2 extrapolation are consistent with each other, but the former has larger error, due to extrapolating over a larger range of numerical distance to zero. The error in the light-nucleon extrapolated RpITD values is consistently double that of the strange nucleon.

B. Continuum-physical extrapolation

We extrapolate the nucleon gluon PDF at the physical pion mass and continuum limit based on the RpITDs for the

a12m220, a09m310, a12m310, and a15m310 ensembles. Given that we observe small differences between a and a^2 extrapolation at fixed M_π and ν in the previous subsection, we focus on a^2 extrapolation here. We use the following ansatz, linear in pion mass and lattice-spacing squared, to extrapolate to the continuum-physical limit:

$$\mathcal{M}(\nu, z^2, a, M_\pi) = \left(\sum_{k=0}^{k_{\rm max}} \lambda_k(a, M_\pi)\nu^k + c_z(a, M_\pi)z^2 \right)$$
$$\times (1 + c_a a^2 + c_M(M_\pi^2 - (M_\pi^{\rm phys})^2)), \quad (9)$$

Given the noisiness of the gluon RpITD data, $k_{\rm max} = 2$ is used in this study. The goodness of fit is around 0.5. We found that in all the ensembles in our calculation, the z^2-dependence, $c_z(a, M_\pi)$ is consistent with zero within two standard deviations. The example reconstructed fitted bands for a09m310 and a12m220 are shown in the top plot of Fig. 5. We drop data points at a ν value if they have errors
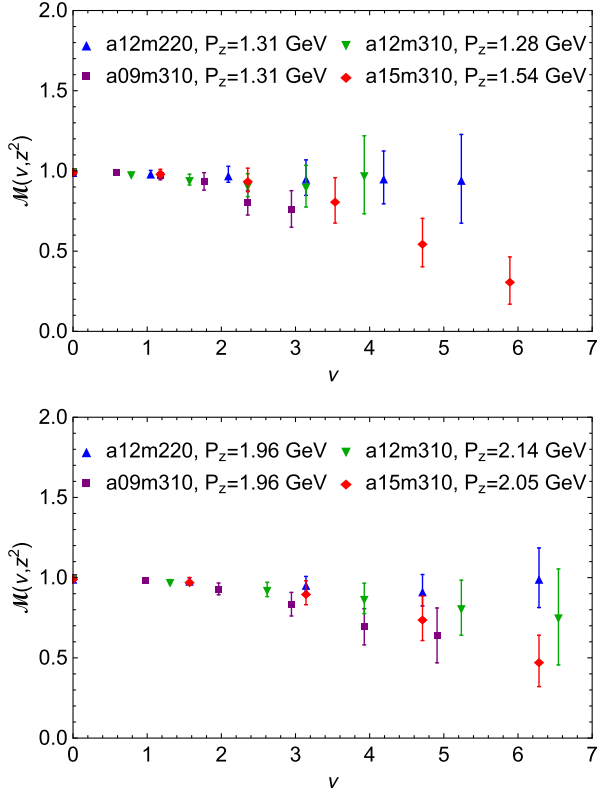
FIG. 3. The RpITDs at boost momenta $P_z \approx 1.3$ GeV (top) and 2 GeV (bottom) as functions of Ioffe-time ν obtained from the fitted bare ground-state matrix elements for $M_\pi \approx \{220, 310, 310, 310\}$ MeV on a12m220, a09m310, a12m310, a15m310 ensembles, respectively. There is no significant lattice-spacing or pion-mass dependence.

more than twice as large another data point at that ν; this improves the clarity of the diagram showing the extrapolation effects. Our fit ansatz is able to describe our data reasonably with ν up to about 7; in the future, when larger P_z is used to reach larger ν, a better interpolation form will likely be needed to describe the small- and large-ν regions well. We show the continuum-physical RpITD band on the top plot of Fig. 5 with all the data points from the four ensembles and a^2 extrapolation to the continuum-physical band. The open symbols indicate the strange-mass nucleon calculation from the ensemble. With the a15m310, a12m310, and a09m310 ensembles, since we have the same number of measurements for both strange and light nucleons, within each ensemble we bootstrap the light and strange renormalized matrix elements to keep the correlations. Across the ensembles, the data are independent and the typical bootstrap treatment is used. For comparison purposes, we also replace the a^2 term in Eq. (9) with a, which causes the goodness of fit to shift by 0.05; its physical-continuum results are shown as the band with dashed center line in Fig. 5. Similar to what we observe in Fig. 4, both extrapolations give us a consistent continuum-physical limit (within one standard deviation) with Ioffe time ν up to 7, but the $O(a)$-extrapolated continuum-physical RpITD has larger errors, especially in the larger-ν region.

C. Gluon PDF results

With the physical-continuum RpITD obtained in the previous section, we can now extract the gluon PDF distribution using the pseudo-PDF matching condition [105] that connects the RpITD $\mathcal{M}$ to the lightcone
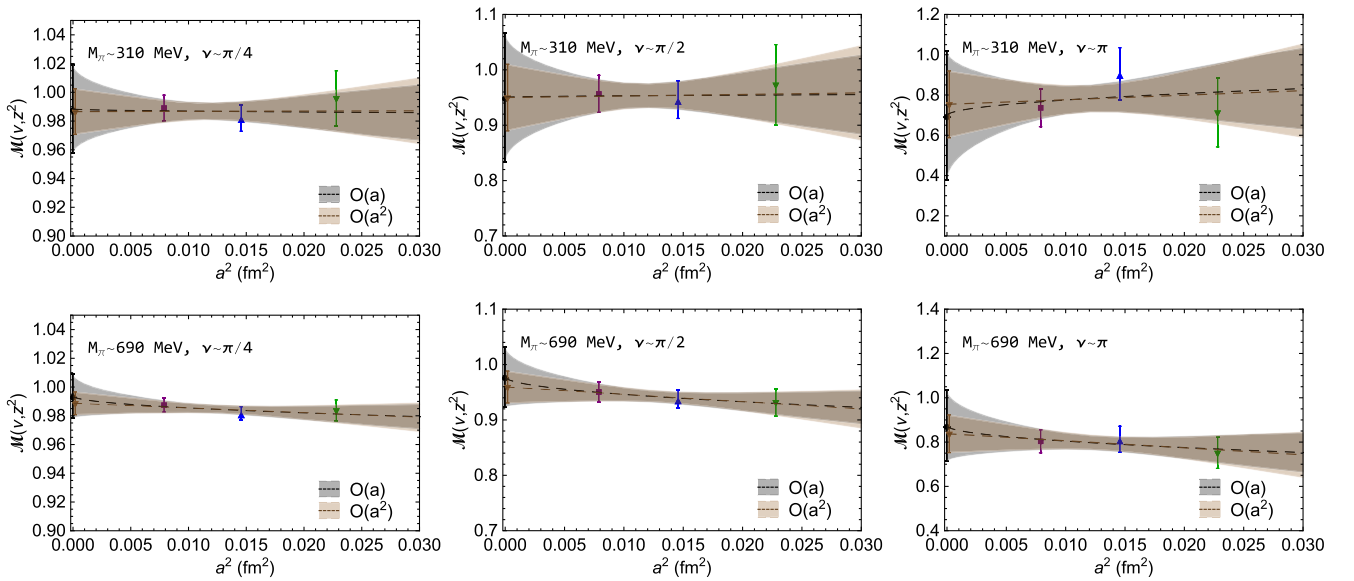

FIG. 4. RpITDs and the reconstructed bands from $O(a)$ or $O(a^2)$ fits of three lattice spacings for a09m310, a12m310, and a15m310 ensembles from left to right panel respectively, for both light (top row) and strange nucleons (bottom row) at $\nu = \{\pi/4, \pi/2, \pi\}$.
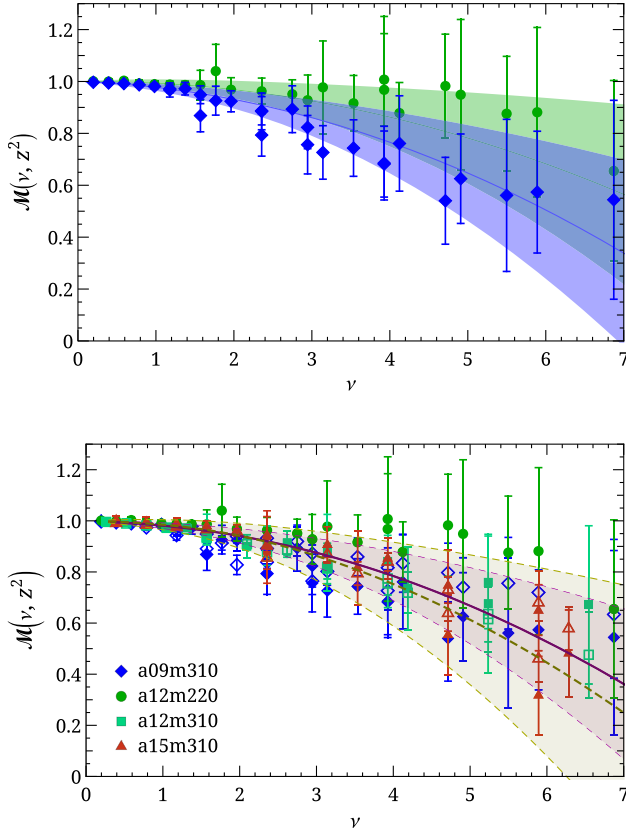
FIG. 5. Top: examples of the RpITDs $\mathcal{M}$ reconstructed bands from fits in Eq. (9) for a09m310 (blue points and light blue band), a12m220 (green) lattice ensembles. The fit ansatz is able to describe the data well. Bottom: Collected data for all ensembles with a (dashed band) and a^2 (solid band) continuum extrapolation at the physical pion mass. Open symbols indicates the data point from the same-symbol ensemble but at the heavier quark mass.

gluon PDF $g(x, \mu^2)$:

$$\mathcal{M}(\nu, z^2) = \int_0^1 dx \frac{xg(x, \mu^2)}{\langle x \rangle_g} R_{gg}(x\nu, z^2\mu^2), \quad (10)$$

where μ is the renormalization scale in the $\overline{\text{MS}}$ scheme and $\langle x \rangle_g = \int_0^1 dx \, xg(x, \mu^2)$ is the gluon momentum fraction of the nucleon. R_{gg} is the gluon-in-gluon matching kernel originally derived in Ref. [105] and has been used in previous gluon PDF lattice works [92,95,96,104]. We use the RpITD extrapolated using the a^2 term [in Eq. (12)] at physical pion mass and continuum limit with a fit range of $\nu \in [0, 7]$, corresponding to the region where we have data in all ensembles. We ignore the quark-PDF contribution to the RpITDs in this calculation; it is likely to be small, based on our past study of the pion gluon PDF [96]. We will later estimate the quark contribution as a systematic effect. One can obtain the gluon PDF $g(x, \mu^2)$ by fitting the RpITD through the matching condition in Eq. (10). We adopt the

phenomenologically motivated form commonly used in global analyses

$$f_g(x, \mu) = \frac{xg(x, \mu)}{\langle x \rangle_g(\mu)} = \frac{x^A(1-x)^C}{B(A+1, C+1)}, \quad (11)$$

for $x \in [0, 1]$ and zero elsewhere. The beta function $B(A+1, C+1) = \int_0^1 dx \, x^A(1-x)^C$ is used to normalize the area to unity. Such a form is also used in global fits, such as that of the nucleon gluon PDF by CT18 [7] and the nucleon and pion gluon PDF by JAM [129–131]. We then fit the lattice physical-continuum RpITDs $\mathcal{M}^{\text{lat}}(\nu, z^2, a, M_\pi)$ obtained in Eq. (9) to the parametrization form $\mathcal{M}^{\text{fit}}(\nu, \mu, z^2, a, M_\pi)$ in Eq. (10) by minimizing the χ^2 function,

$$\chi^2(\mu, a, M_\pi)$$
$$= \sum_{\nu, z} \frac{(\mathcal{M}^{\text{fit}}(\nu, \mu, z^2, a, M_\pi) - \mathcal{M}^{\text{lat}}(\nu, z^2, a, M_\pi))^2}{\sigma_{\mathcal{M}}^2(\nu, z^2, a, M_\pi)}.$$
$$(12)$$

Our results for the continuum-physical unpolarized gluon PDF $xg(x, \mu)/\langle x \rangle_g$ are shown in Fig. 6, along with the same determination from the smallest lattice-spacing ensemble obtained in this work, and selected global-fit gluon PDFs from CT18 [7] and NNPDF3.1 [6] NNLO analysis. The gluon distribution in continuum-physical limit has much larger errors by a factor of 3–5 than those obtained from single–lattice-spacing analysis, due to the continuum extrapolation. Overall, the results from single-ensemble calculations on a09m310 are consistent with the continuum-physical one (which has much larger uncertainties). To reduce the errors in the continuum-physical distribution will be difficult, since it requires reduced errors in all ensembles, increasing the calculation cost by at least another order of magnitude. Both of our lattice distributions agree with the global-fit gluon distribution at mid to large x but deviate for $x < 0.3$. This is likely due to lack of large-ν lattice data in the input, which has higher sensitivity to the smaller-x data. Future calculations to push for even larger P_z will be needed to improve the small-x gluon distribution.

We now consider the systematic uncertainty coming from neglecting the contribution of the quark term, $\frac{P_z}{P_0} \int_0^1 dx \frac{xq_S(x, \mu^2)}{\langle x \rangle_g} R_{gq}(x\nu, z^2\mu^2)$ in Eq. (10). We ignored this contribution initially based on the assumption (motivated by global fits) that the nucleon total quark PDF $q_S(x)$ is smaller than the gluon PDF. We can estimate the systematic due to omitting the $q_S(x)$ contribution by using the nucleon flavor-dependent quark PDFs from CT18 at NNLO [7]. Following a similar procedure to Ref. [96], we add the quark-gluon mixing term to the extraction of $xg(x)/\langle x \rangle_g$ from the RpITD in Eq. (10). The central value of the updated $xg(x)/\langle x \rangle_g$ including both gluon-in-gluon (gg) and gluon-in-quark (gq) contributions is shown in Fig. 6 (black solid line). The difference is much smaller than the current
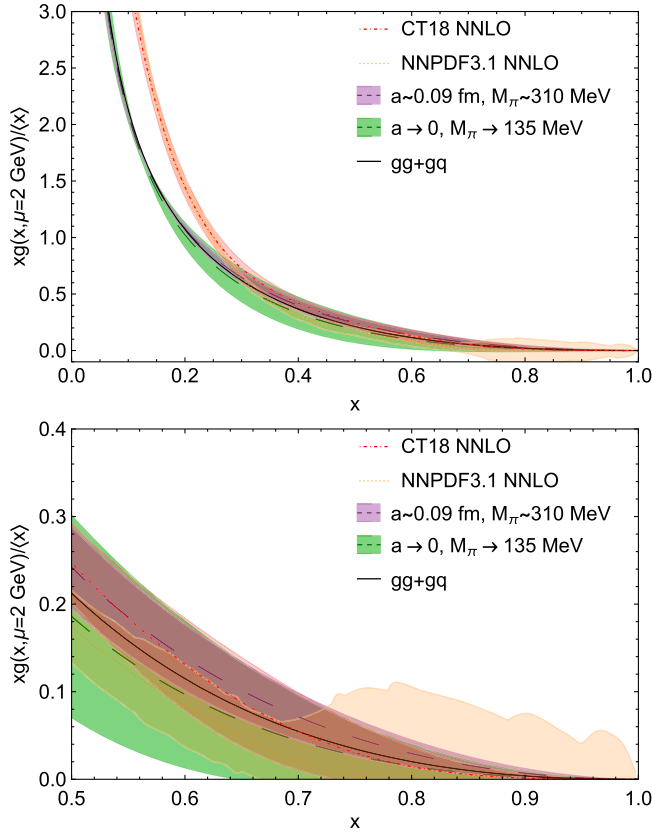
FIG. 6. The unpolarized gluon PDF, $xg(x,\mu)/\langle x \rangle_g$ as a function of x and its zoomed in plot, obtained from the fits to the smallest–lattice-spacing ensemble data compared with the fit to the data obtained from extrapolation to physical pion mass and continuum limit. The black solid line is the central value of the fit to the continuum-physical PDFs, including the gluon-in-quark term in the matching, using CT18 for the quark PDF contributions. The results from the global fits by CT18 [7] and NNPDF3.1 [6] NNLO gluon PDFs are also shown in the plots, and our gluon PDF results are consistent with the global fits for $x \in [0.3, 1]$.

statistical errors, so we will ignore this quark contribution in this calculation. However, in the future, when the continuum-physical gluon PDF precision are improved, we should reexamine this contribution more carefully.

We investigate the systematic uncertainty introduced by the choice of parametrization form used for $f_g(x,\mu)$. We consider a three-parameter form used in PDF global analysis and some lattice calculations,

$$f_{g,3}(x,\mu) = \frac{x^A(1-x)^C(1+Dx)}{B(A+1,C+1) + DB(A+2,C+1)}. \quad (13)$$

We fit our continuum-physical–limit RpITDs to this form up to maximal Ioffe time $\nu_{\max} = 7$. A comparison of the fit-form choice is shown in Fig. 7. We find the goodness-of-fit improves slightly due to the introduction of a new free parameter in the fit form, but the gluon PDF results are noisier and are consistent with the two-parameter fit.
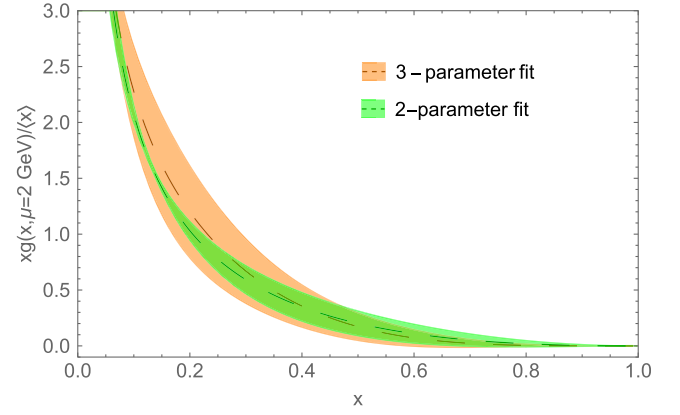

FIG. 7. $xg(x,\mu)/\langle x \rangle_g$ at $\mu^2 = 4$ GeV^2 as function of x, extracted from continuum-physical RpITDs using the two- (green) and three-parameter (orange) fits described in Eqs. (11) and (13), respectively. The results are consistent within statistical errors.

We will use $xg(x,\mu)/\langle x \rangle_g$ from the two-parameter fit as our main result for this work.

The unpolarized nucleon gluon PDF $xg(x)$ can be extracted by taking the ratio of $f_g(x,\mu) = xg(x,\mu)/\langle x \rangle_g(\mu)$ and the gluon momentum fraction $\langle x \rangle_g(\mu)$ obtained in Ref. [132]. Reference [132] calculated the gluon momentum fraction using valence clover fermion action on 0.09-, 0.12-, and 0.15-fm HISQ $2+1+1$-flavor lattice ensembles with three pion masses, 220, 310, and 690 MeV. The renormalization was done using RI/MOM nonperturbative renormalization in $\overline{\text{MS}}$ scheme at 2 GeV and using cluster-decomposition error reduction (CDER) to enhance the signal-to-noise ratio of the renormalization constant [133,134]. The gluon momentum fraction was extrapolated to the continuum-physical limit and found to be consistent with other recent lattice-QCD results at physical pion mass. Our final unpolarized nucleon gluon PDF $xg(x)$ extrapolated to physical pion mass $M_\pi = 135$ MeV and the continuum limit $a \to 0$ is shown as green bands in Fig. 8. Once again, we find reasonable agreement with the global fits from CT18 [7] and NNPDF3.1 [6] NNLO analysis for $x \in [0.25, 1]$, even though the gluon momentum fraction obtained from the global fits is about two sigma lower than the lattice calculations. We do observe tension with the gluon PDF from JAM20 [129] for $x < 0.6$, but its gluon PDF also behaves quite differently from the CT18 and NNPDF results, even with smaller errors. We look forward to updates by the global-fit community to resolve this discrepancy.

We also compare our results with previous lattice-QCD calculations of $xg(x)$. The cyan bands in Fig. 8 show the first pseudo-PDF calculation done using clover-on-HISQ with 0.12-fm lattice spacing and 310- and 700-MeV pion mass using 898 lattice configurations with 32 sources per configuration for the nucleon two-point correlators [92]. The results are extrapolated to physical pion mass using
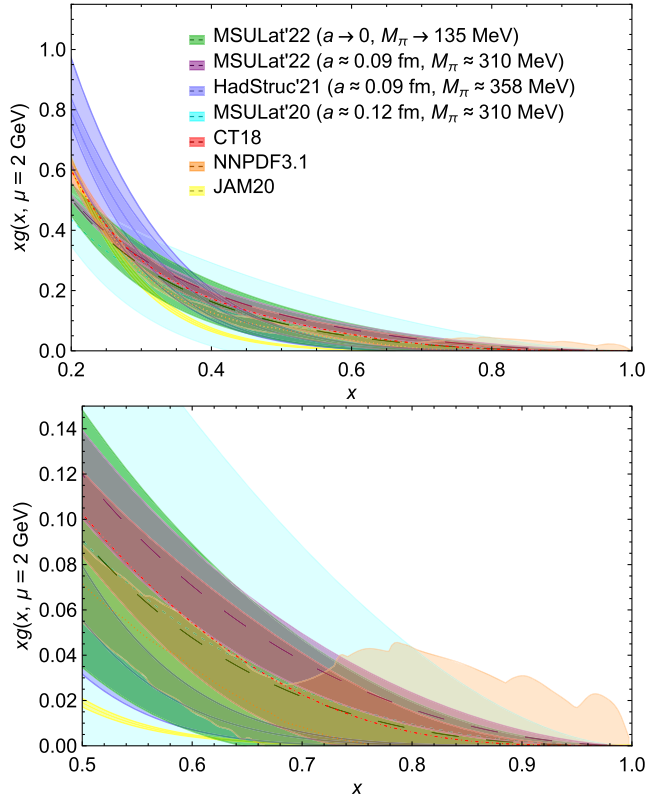
FIG. 8. The unpolarized gluon PDF, $xg(x,\mu)$ a function of x with $x \in [0.2, 1]$ (top) region as and a close-look of the large-x region (bottom), obtained from our continuum-physical (green) and a09m310-ensemble (purple) RpITDs compared with a single-ensemble analysis from HadStruc ($a \approx 0.094$ fm, $M_\pi \approx 358$ MeV), and the CT18 NNLO [7] (red band), NNPDF3.1 NNLO [6] (orange ban), and JAM20 [129] (yellow band) gluon PDFs at $\mu = 2$ GeV in the $\overline{\text{MS}}$ scheme. Other prior lattice calculations of $xg(x)$ (including those done at single ensemble) from HadStruc [95] (blue band) and MSULat [92] (cyan band) are also shown in the plot. Our PDF results are consistent with the CT18 NNLO and NNPDF3.1 NNLO unpolarized gluon PDFs within errors.

naive extrapolation of the two valence pion masses with $xg(x)$ reconstructed by multiplying the gluon momentum fraction taken from Ref. [55]. The blue bands in Fig. 8 show a followup calculation performed by HadStruc Collaboration using $2 + 1$ dynamical flavors of clover fermions with stout-link smearing on the gauge fields, 0.09-fm lattice spacing, 358-MeV pion mass, and 64 source measurements on 349 lattice configurations with gradient-flow improved gluonic operators [95]. They used multiple nucleon interpolating fields, allowing them to use generalized eigenvalue method to determine the best overlap with ground-state nucleon gluonic matrix elements. They used the gluon momentum fraction obtained from an independent lattice work ($2 + 1 + 1$-flavor at physical pion mass) to determine $xg(x)$. The outer blue bands indicate their uncertainty estimated from $\langle x \rangle_g$. We also show our

result on the ensemble with 0.09-fm lattice-spacing and 310-MeV pion mass as a purple band in Fig. 8; it used about 300 k measurements spread out over 1000 lattice configurations. Our single-ensemble results have errors comparable to (in some regions, smaller than) CT18 and NNPDF. The lattice-spacing and pion-mass here is similar to those used in the HadStruc calculation [95] but without the additional uncertainties due to continuum-physical extrapolation (shown as a green band). There are noticeable deviations from the HadStruc results, especially in the larger-x region; their large-x gluon PDF is much smaller than ours. However, given that multiple methodological aspects are done quite differently (for example, we used the momentum fraction from the same lattice ensemble and different gluon-operator smearing), it may require the full calculation, including continuum-physical extrapolation, to meaningfully compare them. All the prior single-ensemble lattice results (without the systematics from lattice discretization) agree with our continuum-physical $xg(x)$ due to the larger total errors from the continuum-physical extrapolation. Future work to include finer lattice-spacing and 220-MeV or lighter pion masses in the extrapolation will help to improve the continuum-physical determination of the lattice gluon PDF.

IV. SUMMARY AND OUTLOOK

We extracted the nucleon x-dependent gluon PDFs $xg(x)$ using clover fermions as valence action and $2 + 1 + 1$ HISQ configurations generated by the MILC Collaboration at three pion masses and three lattice spacings. We found their dependence to be weak at the current statistics of hundreds of thousands of nucleon two-point correlator measurements. We removed the excited-state contributions to the ground-state matrix elements using a two-state fitting strategy and studied the stability of the extraction of the ground-state matrix elements with various fit ranges. We then calculated the reduced pseudo-ITD using the fitted matrix elements and studied their pion-mass and lattice-spacing dependence, which are also mild. We then extrapolated the reduced pseudo-ITDs to physical-continuum limit before extracting the gluon parton distribution $xg(x)/\langle x \rangle_g$ in the $\overline{\text{MS}}$ scheme at 2 GeV. Using the nonperturbatively renormalized nucleon momentum fraction calculated on clover-on-HISQ ensembles, we were able to compare our single-ensemble $xg(x)$ calculations at lattice spacing 0.09 fm with prior lattice calculations. We found both our 0.09-fm and continuum-physical limit $xg(x)$ to be in good agreement with CT18 and NNPDF3.1 NNLO global-fit results in the range $x \in [0.2, 1]$ in $\overline{\text{MS}}$ scheme at 2 GeV. We have used the CT18 quark PDFs to estimate the quark-gluon mixing and checked the gluon PDF fit-form dependence, but these errors are not included in our continuum-physical results, since the statistical errors are large in comparison. Future work should include finer

[1] L. A. Harland-Lang, A. D. Martin, P. Motylinski, and R. S. Thorne, Parton distributions in the LHC era: MMHT 2014 PDFs, Eur. Phys. J. C **75**, 204 (2015).

[2] Sayipjamal Dulat, Tie-Jiun Hou, Jun Gao, Marco Guzzi, Joey Huston, Pavel Nadolsky, Jon Pumplin, Carl Schmidt, Daniel Stump, and C. P. Yuan, New parton distribution functions from a global analysis of quantum chromodynamics, Phys. Rev. D **93**, 033006 (2016).

[3] H. Abramowicz et al., Combination of measurements of inclusive deep inelastic $e^{\pm}p$ scattering cross sections and QCD analysis of HERA data, Eur. Phys. J. C **75**, 580 (2015).

[4] A. Accardi, L. T. Brady, W. Melnitchouk, J. F. Owens, and N. Sato, Constraints on large-x parton distributions from new weak boson production and deep-inelastic scattering data, Phys. Rev. D **93**, 114017 (2016).

[5] S. Alekhin, J. Blümlein, S. Moch, and R. Placakyte, Parton distribution functions, α_s, and heavy-quark masses for LHC Run II, Phys. Rev. D **96**, 014011 (2017).

[6] Richard D. Ball et al., Parton distributions from high-precision collider data, Eur. Phys. J. C **77**, 663 (2017).

[7] Tie-Jiun Hou et al., New CTEQ global analysis of quantum chromodynamics with high-precision data from the LHC, Phys. Rev. D **103**, 014013 (2021).

[8] Shaun Bailey and Lucian Harland-Lang, Differential top quark pair production at the LHC: Challenges for PDF fits, Eur. Phys. J. C **80**, 60 (2020).

[9] S. Bailey, T. Cridge, L. A. Harland-Lang, A. D. Martin, and R. S. Thorne, Parton distributions from LHC, HERA, Tevatron and fixed target data: MSHT20 PDFs, Eur. Phys. J. C **81**, 341 (2021).

[10] Richard D. Ball et al., The path to proton structure at 1% accuracy, Eur. Phys. J. C **82**, 428 (2022).

[11] Georges Aad et al., Determination of the parton distribution functions of the proton using diverse ATLAS data from pp collisions at $\sqrt{s} = 7$, 8 and 13 TeV, Eur. Phys. J. C **82**, 438 (2022).

[12] Serguei Chatrchyan et al., A new boson with a mass of 125 GeV observed with the CMS experiment at the large hadron collider, Science **338**, 1569 (2012).

[13] Roman Kogler et al., Jet substructure at the Large Hadron Collider: Experimental review, Rev. Mod. Phys. **91**, 045003 (2019).

[14] J. Mammei, S. Riordan, K. Kumar, J. Wexler, K. Paschke, G. D. Cates, M. Dalton, X. Zheng, P. A. Souder, R. Holmes et al., Proposal to Jefferson Lab PAC 39.

[15] A. Accardi et al., Electron ion collider: The next QCD frontier: Understanding the glue that binds us all, Eur. Phys. J. A **52**, 268 (2016).

[16] J. Arrington et al., Revealing the structure of light pseudoscalar mesons at the electron-ion collider, J. Phys. G **48**, 075106 (2021).

[17] Arlene C. Aguilar et al., Pion and kaon structure at the electron-ion collider, Eur. Phys. J. A **55**, 190 (2019).

[18] R. Abdul Khalek et al., Science requirements and detector concepts for the electron-ion collider: EIC yellow report, Nucl. Phys. **A1026**, 122447 (2022).

[19] Daniele P. Anderle et al., Electron-ion collider in China, Front. Phys. (Beijing) **16**, 64701 (2021).

[20] Xiangdong Ji, Parton Physics on a Euclidean Lattice, Phys. Rev. Lett. **110**, 262002 (2013).

[21] Xiangdong Ji, Parton physics from large-momentum effective field theory, Sci. China Phys. Mech. Astron. **57**, 1407 (2014).

[22] Xiangdong Ji, Jian-Hui Zhang, and Yong Zhao, More on large-momentum effective theory approach to parton physics, Nucl. Phys. **B924**, 366 (2017).

[23] Huey-Wen Lin, Calculating the x dependence of hadron parton distribution functions, Proc. Sci. LATTICE2013 (**2014**) 293.

[24] Huey-Wen Lin, Jiunn-Wei Chen, Saul D. Cohen, and Xiangdong Ji, Flavor structure of the nucleon sea from lattice QCD, Phys. Rev. D **91**, 054510 (2015).

[25] Jiunn-Wei Chen, Saul D. Cohen, Xiangdong Ji, Huey-Wen Lin, and Jian-Hui Zhang, Nucleon helicity and transversity parton distributions from lattice QCD, Nucl. Phys. **B911**, 246 (2016).

[26] Huey-Wen Lin, Jiunn-Wei Chen, Tomomi Ishikawa, and Jian-Hui Zhang, Improved parton distribution functions at the physical pion mass, Phys. Rev. D **98**, 054504 (2018).

[27] Constantia Alexandrou, Krzysztof Cichy, Vincent Drach, Elena Garcia-Ramos, Kyriakos Hadjiyiannakou, Karl Jansen, Fernanda Steffens, and Christian Wiese, Lattice calculation of parton distributions, Phys. Rev. D **92**, 014502 (2015).

[28] Constantia Alexandrou, Krzysztof Cichy, Martha Constantinou, Kyriakos Hadjiyiannakou, Karl Jansen, Fernanda Steffens, and Christian Wiese, Updated lattice results for parton distributions, Phys. Rev. D **96**, 014513 (2017).

[29] Constantia Alexandrou, Krzysztof Cichy, Martha Constantinou, Kyriakos Hadjiyiannakou, Karl Jansen, Haralambos Panagopoulos, and Fernanda Steffens, A complete non-perturbative renormalization prescription for quasi-PDFs, Nucl. Phys. **B923**, 394 (2017).

[30] Jiunn-Wei Chen, Tomomi Ishikawa, Luchang Jin, Huey-Wen Lin, Yi-Bo Yang, Jian-Hui Zhang, and Yong Zhao, Parton distribution function with nonperturbative renormalization from lattice QCD, Phys. Rev. D **97**, 014505 (2018).

[31] Constantia Alexandrou, Krzysztof Cichy, Martha Constantinou, Karl Jansen, Aurora Scapellato, and Fernanda Steffens, Light-Cone Parton Distribution Functions from Lattice QCD, Phys. Rev. Lett. **121**, 112001 (2018).

[32] Jiunn-Wei Chen, Luchang Jin, Huey-Wen Lin, Yu-Sheng Liu, Yi-Bo Yang, Jian-Hui Zhang, and Yong Zhao, Lattice calculation of parton distribution function from LaMET at physical pion mass with large nucleon momentum, arXiv:1803.04393.

[33] Jian-Hui Zhang, Jiunn-Wei Chen, Luchang Jin, Huey-Wen Lin, Andreas Schäfer, and Yong Zhao, First direct lattice-QCD calculation of the x-dependence of the pion parton distribution function, Phys. Rev. D **100**, 034505 (2019).

[34] Constantia Alexandrou, Krzysztof Cichy, Martha Constantinou, Karl Jansen, Aurora Scapellato, and Fernanda Steffens, Transversity parton distribution functions from lattice QCD, Phys. Rev. D **98**, 091503 (2018).

[35] Huey-Wen Lin, Jiunn-Wei Chen, Xiangdong Ji, Luchang Jin, Ruizi Li, Yu-Sheng Liu, Yi-Bo Yang, Jian-Hui Zhang, and Yong Zhao, Proton Isovector Helicity Distribution on the Lattice at Physical Pion Mass, Phys. Rev. Lett. **121**, 242003 (2018).

[36] Zhou-You Fan, Yi-Bo Yang, Adam Anthony, Huey-Wen Lin, and Keh-Fei Liu, Gluon Quasi-Parton-Distribution Functions from Lattice QCD, Phys. Rev. Lett. **121**, 242001 (2018).

[37] Yu-Sheng Liu, Jiunn-Wei Chen, Luchang Jin, Ruizi Li, Huey-Wen Lin, Yi-Bo Yang, Jian-Hui Zhang, and Yong Zhao, Nucleon transversity distribution at the physical pion mass from lattice QCD, arXiv:1810.05043

[38] Wei Wang, Jian-Hui Zhang, Shuai Zhao, and Ruilin Zhu, Complete matching for quasidistribution functions in large momentum effective theory, Phys. Rev. D **100**, 074509 (2019).

[39] Huey-Wen Lin and Rui Zhang, Lattice finite-volume dependence of the nucleon parton distributions, Phys. Rev. D **100**, 074502 (2019).

[40] Jiunn-Wei Chen, Huey-Wen Lin, and Jian-Hui Zhang, Pion generalized parton distribution from lattice QCD, Nucl. Phys. **B952**, 114940 (2020).

[41] Huimei Liu, Frontiers in lattice nucleon structure, Int. J. Mod. Phys. A **35**, 2030006 (2020).

[42] Yahui Chai et al., Parton distribution functions of Δ^+ on the lattice, Phys. Rev. D **102**, 014508 (2020).

[43] Shohini Bhattacharya, Krzysztof Cichy, Martha Constantinou, Andreas Metz, Aurora Scapellato, and Fernanda Steffens, Insights on proton structure from lattice QCD: The twist-3 parton distribution function $g_T(x)$, Phys. Rev. D **102**, 111501 (2020).

[44] Huey-Wen Lin, Jiunn-Wei Chen, Zhouyou Fan, Jian-Hui Zhang, and Rui Zhang, Valence-quark distribution of the kaon and pion from lattice QCD, Phys. Rev. D **103**, 014516 (2021).

[45] Rui Zhang, Huey-Wen Lin, and Boram Yoon, Probing nucleon strange and charm distributions with lattice QCD, Phys. Rev. D **104**, 094511 (2021).

[46] Zheng-Yang Li, Yan-Qing Ma, and Jian-Wei Qiu, Extraction of Next-to-Next-to-Leading-Order Parton Distribution Functions from Lattice QCD Calculations, Phys. Rev. Lett. **126**, 072001 (2021).

[47] Zhouyou Fan, Xiang Gao, Ruizi Li, Huey-Wen Lin, Nikhil Karthik, Swagato Mukherjee, Peter Petreczky, Sergey Syritsyn, Yi-Bo Yang, and Rui Zhang, Isovector parton distribution functions of the proton on a superfine lattice, Phys. Rev. D **102**, 074504 (2020).

[48] Xiang Gao, Luchang Jin, Christos Kallidonis, Nikhil Karthik, Swagato Mukherjee, Peter Petreczky, Charles Shugert, Sergey Syritsyn, and Yong Zhao, Valence parton distribution of the pion from lattice QCD: Approaching the continuum limit, Phys. Rev. D **102**, 094513 (2020).

[49] Huey-Wen Lin, Jiunn-Wei Chen, and Rui Zhang, Lattice nucleon isovector unpolarized parton distribution in the physical-continuum limit, arXiv:2011.14971.

[50] Kuan Zhang, Yuan-Yuan Li, Yi-Kai Huo, Andreas Schäfer, Peng Sun, and Yi-Bo Yang, RI/MOM renormalization of the parton quasidistribution functions in lattice regularization, Phys. Rev. D **104**, 074501 (2021).

[51] Constantia Alexandrou, Krzysztof Cichy, Martha Constantinou, Jeremy R. Green, Kyriakos Hadjiyiannakou, Karl Jansen, Floriano Manigrasso, Aurora Scapellato, and Fernanda Steffens, Lattice continuum-limit study of nucleon quasi-PDFs, Phys. Rev. D **103**, 094512 (2021).

[52] Constantia Alexandrou, Krzysztof Cichy, Martha Constantinou, Kyriakos Hadjiyiannakou, Karl Jansen, Aurora Scapellato, and Fernanda Steffens, Unpolarized and Helicity Generalized Parton Distributions of the Proton within Lattice QCD, Phys. Rev. Lett. **125**, 262001 (2020).

[53] Huey-Wen Lin, Nucleon Tomography and Generalized Parton Distribution at Physical Pion Mass from Lattice QCD, Phys. Rev. Lett. **127**, 182001 (2021).

[54] Xiang Gao, Kyle Lee, Swagato Mukherjee, Charles Shugert, and Yong Zhao, Origin and resummation of threshold logarithms in the lattice QCD calculations of PDFs, Phys. Rev. D **103**, 094504 (2021).

[55] Martha Constantinou et al., Parton distributions and lattice-QCD calculations: Toward 3D structure, Prog. Part. Nucl. Phys. **121**, 103908 (2021).

[56] U. Aglietti, Marco Ciuchini, G. Corbo, E. Franco, G. Martinelli, and L. Silvestrini, Model independent determination of the light cone wave functions for exclusive processes, Phys. Lett. B **441**, 371 (1998).

[57] G. Martinelli, Hadronic weak interactions of light quarks, Nucl. Phys. B, Proc. Suppl. **73**, 58 (1999).

[58] C. Dawson, G. Martinelli, G. C. Rossi, Christopher T. Sachrajda, Stephen R. Sharpe, M. Talevi, and M. Testa, New lattice approaches to the delta I = 1/2 rule, Nucl. Phys. **B514**, 313 (1998).

[59] S. Capitani, M. Gockeler, R. Horsley, H. Oelrich, D. Petters, Paul E. L. Rakow, and G. Schierholz, Towards a nonperturbative calculation of DIS Wilson coefficients, Nucl. Phys. B, Proc. Suppl. **73**, 288 (1999).

[60] S. Capitani, M. Gockeler, R. Horsley, D. Petters, D. Pleiter, Paul E. L. Rakow, and G. Schierholz, Higher twist corrections to nucleon structure functions from lattice QCD, Nucl. Phys. B, Proc. Suppl. **79**, 173 (1999).

[61] Xiang-dong Ji and Chul-woo Jung, Studying Hadronic Structure of the Photon in Lattice QCD, Phys. Rev. Lett. **86**, 208 (2001).

[62] William Detmold and C. J. David Lin, Deep-inelastic scattering and the operator product expansion in lattice QCD, Phys. Rev. D **73**, 014501 (2006).

[63] V. Braun and Dieter Müller, Exclusive processes in position space and the pion distribution amplitude, Eur. Phys. J. C **55**, 349 (2008).

[64] A. J. Chambers, R. Horsley, Y. Nakamura, H. Perlt, P. E. L. Rakow, G. Schierholz, A. Schiller, K. Somfleth, R. D. Young, and J. M. Zanotti, Nucleon Structure Functions from Operator Product Expansion on the Lattice, Phys. Rev. Lett. **118**, 242001 (2017).

[65] William Detmold, Issaku Kanamori, C. J. David Lin, Santanu Mondal, and Yong Zhao, Moments of pion distribution amplitude using operator product expansion on the lattice, Proc. Sci. LATTICE2018 (**2018**) 106.

[66] A. Hannaford-Gunn, R. Horsley, Y. Nakamura, H. Perlt, P. E. L. Rakow, G. Schierholz, K. Somfleth, H. Stüben, R. D. Young, and J. M. Zanotti, Scaling and higher twist in the nucleon Compton amplitude, Proc. Sci. LATTICE2019 (**2020**) 278.

[67] Roger Horsley, Yoshifumi Nakamura, Holger Perlt, Paul E. L. Rakow, Gerrit Schierholz, Kim Somfleth, Ross D. Young, and James M. Zanotti, Structure functions from the Compton amplitude, Proc. Sci. LATTICE2019 (**2020**) 137.

[68] William Detmold, Anthony V. Grebe, Issaku Kanamori, C. J. David Lin, Robert J. Perry, and Yong Zhao, Parton physics from a heavy-quark operator product expansion: Formalism and Wilson coefficients, Phys. Rev. D **104**, 074511 (2021).

[69] Keh-Fei Liu and Shao-Jing Dong, Origin of Difference between $\bar{d}$ and $\bar{u}$ Partons in the Nucleon, Phys. Rev. Lett. **72**, 1790 (1994).

[70] K. F. Liu, S. J. Dong, Terrence Draper, D. Leinweber, J. H. Sloan, W. Wilcox, and R. M. Woloshyn, Valence QCD: Connecting QCD to the quark model, Phys. Rev. D **59**, 112001 (1999).

[71] Keh-Fei Liu, Parton degrees of freedom from the path integral formalism, Phys. Rev. D **62**, 074501 (2000).

[72] Keh-Fei Liu, Parton distribution function from the hadronic tensor on the lattice, Proc. Sci. LATTICE2015 (**2016**) 115.

[73] Keh-Fei Liu, Evolution equations for connected and disconnected sea parton distributions, Phys. Rev. D **96**, 033001 (2017).

[74] Keh-Fei Liu, PDF in PDFs from hadronic tensor and LaMET, Phys. Rev. D **102**, 074502 (2020).

[75] Yan-Qing Ma and Jian-Wei Qiu, Exploring Partonic Structure of Hadrons Using *ab initio* Lattice QCD Calculations, Phys. Rev. Lett. **120**, 022003 (2018).

[76] Gunnar S. Bali *et al.*, Pion distribution amplitude from Euclidean correlation functions, Eur. Phys. J. C **78**, 217 (2018).

[77] Gunnar S. Bali, Vladimir M. Braun, Benjamin Gläßle, Meinulf Göckeler, Michael Gruber, Fabian Hutzler, Piotr Korcyl, Andreas Schäfer, Philipp Wein, and Jian-Hui Zhang, Pion distribution amplitude from Euclidean correlation functions: Exploring universality and higher-twist effects, Phys. Rev. D **98**, 094507 (2018).

[78] Bálint Joó, Joseph Karpie, Kostas Orginos, Anatoly V. Radyushkin, David G. Richards, and Savvas Zafeiropoulos, Parton Distribution Functions from Ioffe Time Pseudodistributions from Lattice Calculations: Approaching the Physical Point, Phys. Rev. Lett. **125**, 232003 (2020).

[79] Raza Sabbir Sufian, Joseph Karpie, Colin Egerer, Kostas Orginos, Jian-Wei Qiu, and David G. Richards, Pion valence quark distribution from matrix element calculated in lattice QCD, Phys. Rev. D **99**, 074507 (2019).

[80] Raza Sabbir Sufian, Colin Egerer, Joseph Karpie, Robert G. Edwards, Bálint Joó, Yan-Qing Ma, Kostas Orginos, Jian-Wei Qiu, and David G. Richards, Pion valence quark distribution from current-current correlation in lattice QCD, Phys. Rev. D **102**, 054508 (2020).

[81] A. V. Radyushkin, Quasi-parton distribution functions, momentum distributions, and pseudo-parton distribution functions, Phys. Rev. D **96**, 034025 (2017).

[82] Kostas Orginos, Anatoly Radyushkin, Joseph Karpie, and Savvas Zafeiropoulos, Lattice QCD exploration of parton pseudo-distribution functions, Phys. Rev. D **96**, 094503 (2017).

[83] Joseph Karpie, Kostas Orginos, Anatoly Radyushkin, and Savvas Zafeiropoulos, Parton distribution functions on the lattice and in the continuum, EPJ Web Conf. **175**, 06032 (2018).

[84] Joseph Karpie, Kostas Orginos, and Savvas Zafeiropoulos, Moments of Ioffe time parton distribution functions from non-local matrix elements, J. High Energy Phys. 11 (2018) 178.

[85] Joseph Karpie, Kostas Orginos, Alexander Rothkopf, and Savvas Zafeiropoulos, Reconstructing parton distribution functions from Ioffe time data: From Bayesian methods to neural networks, J. High Energy Phys. 04 (2019) 057.

[86] Bálint Joó, Joseph Karpie, Kostas Orginos, Anatoly Radyushkin, David Richards, and Savvas Zafeiropoulos, Parton distribution functions from Ioffe time pseudo-distributions, J. High Energy Phys. 12 (2019) 081.

[87] Bálint Joó, Joseph Karpie, Kostas Orginos, Anatoly V. Radyushkin, David G. Richards, Raza Sabbir Sufian, and Savvas Zafeiropoulos, Pion valence structure from

Ioffe-time parton pseudodistribution functions, Phys. Rev. D **100**, 114512 (2019).

[88] Anatoly Radyushkin, One-loop evolution of parton pseudo-distribution functions on the lattice, Phys. Rev. D **98**, 014019 (2018).

[89] Jian-Hui Zhang, Jiunn-Wei Chen, and Christopher Monahan, Parton distribution functions from reduced Ioffe-time distributions, Phys. Rev. D **97**, 074508 (2018).

[90] Taku Izubuchi, Xiangdong Ji, Luchang Jin, Iain W. Stewart, and Yong Zhao, Factorization theorem relating Euclidean and light-cone parton distributions, Phys. Rev. D **98**, 056004 (2018).

[91] Manjunath Bhat, Krzysztof Cichy, Martha Constantinou, and Aurora Scapellato, Flavor nonsinglet parton distribution functions from lattice QCD at physical quark masses via the pseudodistribution approach, Phys. Rev. D **103**, 034510 (2021).

[92] Zhouyou Fan, Rui Zhang, and Huey-Wen Lin, Nucleon gluon distribution function from $2 + 1 + 1$-flavor lattice QCD, Int. J. Mod. Phys. A **36**, 2150080 (2021).

[93] Raza Sabbir Sufian, Tianbo Liu, and Arpon Paul, Gluon distributions and their applications to Ioffe-time distributions, Phys. Rev. D **103**, 036007 (2021).

[94] Nikhil Karthik, Quark distribution inside a pion in many-flavor $(2 + 1)$-dimensional QCD using lattice computations: UV listens to IR, Phys. Rev. D **103**, 074512 (2021).

[95] Tanjib Khan *et al.*, Unpolarized gluon distribution in the nucleon from lattice quantum chromodynamics, Phys. Rev. D **104**, 094516 (2021).

[96] Zhouyou Fan and Huey-Wen Lin, Gluon parton distribution of the pion from lattice QCD, Phys. Lett. B **823**, 136778 (2021).

[97] Colin Egerer *et al.*, Towards the determination of the gluon helicity distribution in the nucleon from lattice quantum chromodynamics, Phys. Rev. D **106**, 094511 (2022).

[98] Xiaonu Xiong, Xiangdong Ji, Jian-Hui Zhang, and Yong Zhao, One-loop matching for parton distributions: Non-singlet case, Phys. Rev. D **90**, 014051 (2014).

[99] Yan-Qing Ma and Jian-Wei Qiu, Extracting parton distribution functions from lattice QCD calculations, Phys. Rev. D **98**, 074021 (2018).

[100] Xiangdong Ji, Yu-Sheng Liu, Yizhuang Liu, Jian-Hui Zhang, and Yong Zhao, Large-momentum effective theory, Rev. Mod. Phys. **93**, 035005 (2021).

[101] Xiang Gao, Andrew D. Hanlon, Swagato Mukherjee, Peter Petreczky, Philipp Scior, Sergey Syritsyn, and Yong Zhao, Lattice QCD Determination of the Bjorken-x Dependence of Parton Distribution Functions at Next-to-Next-to-Leading Order, Phys. Rev. Lett. **128**, 142003 (2022).

[102] Long-Bin Chen, Wei Wang, and Ruilin Zhu, Next-to-Next-to-Leading Order Calculation of Quasiparton Distribution Functions, Phys. Rev. Lett. **126**, 072002 (2021).

[103] Joseph Karpie, Kostas Orginos, Anatoly Radyushkin, and Savvas Zafeiropoulos, The continuum and leading twist limits of parton distribution functions in lattice QCD, J. High Energy Phys. 11 (2021) 024.

[104] Alejandro Salas-Chavira, Zhouyou Fan, and Huey-Wen Lin, First glimpse into the kaon gluon parton distribution using lattice QCD, Phys. Rev. D **106**, 094510 (2022).

[105] Ian Balitsky, Wayne Morris, and Anatoly Radyushkin, Gluon pseudo-distributions at short distances: Forward case, Phys. Lett. B **808**, 135621 (2020).

[106] Jian-Hui Zhang, Xiangdong Ji, Andreas Schäfer, Wei Wang, and Shuai Zhao, Accessing Gluon Parton Distributions in Large Momentum Effective Theory, Phys. Rev. Lett. **122**, 142001 (2019).

[107] E. Follana, Q. Mason, C. Davies, K. Hornbostel, G. P. Lepage, J. Shigemitsu, H. Trottier, and K. Wong, Highly improved staggered quarks on the lattice, with applications to charm physics, Phys. Rev. D **75**, 054502 (2007).

[108] A. Bazavov *et al.*, Lattice QCD ensembles with four flavors of highly improved staggered quarks, Phys. Rev. D **87**, 054505 (2013).

[109] Anna Hasenfratz and Francesco Knechtli, Flavor symmetry and the static potential with hypercubic blocking, Phys. Rev. D **64**, 034504 (2001).

[110] Santanu Mondal, Rajan Gupta, Sungwoo Park, Boram Yoon, Tanmoy Bhattacharya, and Huey-Wen Lin, Moments of nucleon isovector structure functions in $2 + 1 + 1$-flavor QCD, Phys. Rev. D **102**, 054512 (2020).

[111] Sungwoo Park, Tanmoy Bhattacharya, Rajan Gupta, Yong-Chull Jang, Balint Joo, Huey-Wen Lin, and Boram Yoon, Nucleon charges and form factors using clover and HISQ ensembles, Proc. Sci. LATTICE2019 (**2020**) 136.

[112] Yong-Chull Jang, Rajan Gupta, Huey-Wen Lin, Boram Yoon, and Tanmoy Bhattacharya, Nucleon electromagnetic form factors in the continuum limit from $(2 + 1 + 1)$-flavor lattice QCD, Phys. Rev. D **101**, 014507 (2020).

[113] Yong-Chull Jang, Rajan Gupta, Boram Yoon, and Tanmoy Bhattacharya, Axial Vector Form Factors from Lattice QCD that Satisfy the PCAC Relation, Phys. Rev. Lett. **124**, 072002 (2020).

[114] Rajan Gupta, Boram Yoon, Tanmoy Bhattacharya, Vincenzo Cirigliano, Yong-Chull Jang, and Huey-Wen Lin, Flavor diagonal tensor charges of the nucleon from $(2 + 1 + 1)$-flavor lattice QCD, Phys. Rev. D **98**, 091501 (2018).

[115] Huey-Wen Lin, Rajan Gupta, Boram Yoon, Yong-Chull Jang, and Tanmoy Bhattacharya, Quark contribution to the proton spin from $2 + 1 + 1$-flavor lattice QCD, Phys. Rev. D **98**, 094512 (2018).

[116] Rajan Gupta, Yong-Chull Jang, Boram Yoon, Huey-Wen Lin, Vincenzo Cirigliano, and Tanmoy Bhattacharya, Isovector charges of the nucleon from $2 + 1 + 1$-flavor lattice QCD, Phys. Rev. D **98**, 034503 (2018).

[117] Rajan Gupta, Yong-Chull Jang, Huey-Wen Lin, Boram Yoon, and Tanmoy Bhattacharya, Axial vector form factors of the nucleon from lattice QCD, Phys. Rev. D **96**, 114503 (2017).

[118] Rajan Gupta, Yong-Chull Jang, Huey-Wen Lin, Boram Yoon, and Tanmoy Bhattacharya, Axial vector form factors of the nucleon from lattice QCD, Phys. Rev. D **96**, 114503 (2017).

[119] Tanmoy Bhattacharya, Vincenzo Cirigliano, Saul Cohen, Rajan Gupta, Anosh Joseph, Huey-Wen Lin, and Boram Yoon, Iso-vector and iso-scalar tensor charges of the nucleon from lattice QCD, Phys. Rev. D **92**, 094511 (2015).

[120] Tanmoy Bhattacharya, Vincenzo Cirigliano, Rajan Gupta, Huey-Wen Lin, and Boram Yoon, Neutron Electric Dipole

Moment and Tensor Charges from Lattice QCD, Phys. Rev. Lett. **115**, 212002 (2015).

[121] Tanmoy Bhattacharya, Saul D. Cohen, Rajan Gupta, Anosh Joseph, Huey-Wen Lin, and Boram Yoon, Nucleon charges and electromagnetic form factors from $2 + 1 + 1$-flavor lattice QCD, Phys. Rev. D **89**, 094502 (2014).

[122] Andreas S. Kronfeld, David G. Richards, William Detmold, Rajan Gupta, Huey-Wen Lin, Keh-Fei Liu, Aaron S. Meyer, Raza Sufian, and Sergey Syritsyn, Lattice QCD and neutrino-nucleus scattering, Eur. Phys. J. A **55**, 196 (2019).

[123] Huey-Wen Lin *et al.*, Parton distributions and lattice QCD calculations: A community white paper, Prog. Part. Nucl. Phys. **100**, 107 (2018).

[124] Huey-Wen Lin, Hadron spectroscopy and structure from lattice QCD, Few-Body Syst. **63**, 65 (2022).

[125] S. Aoki *et al.*, FLAG review 2019: Flavour lattice averaging group (FLAG), Eur. Phys. J. C **80**, 113 (2020).

[126] Y. Aoki *et al.*, FLAG review 2021, Eur. Phys. J. C **82**, 869 (2022).

[127] Gunnar S. Bali, Bernhard Lang, Bernhard U. Musch, and Andreas Schäfer, Novel quark smearing for hadrons with high momenta in lattice QCD, Phys. Rev. D **93**, 094515 (2016).

[128] Zheng-Yang Li, Yan-Qing Ma, and Jian-Wei Qiu, Multiplicative Renormalizability of Operators Defining Quasiparton Distributions, Phys. Rev. Lett. **122**, 062002 (2019).

[129] Eric Moffat, Wally Melnitchouk, T. C. Rogers, and Nobuo Sato, Simultaneous Monte Carlo analysis of parton densities and fragmentation functions, Phys. Rev. D **104**, 016015 (2021).

[130] P. C. Barry, N. Sato, W. Melnitchouk, and Chueng-Ryong Ji, First Monte Carlo Global QCD Analysis of Pion Parton Distributions, Phys. Rev. Lett. **121**, 152001 (2018).

[131] N. Y. Cao, P. C. Barry, N. Sato, and W. Melnitchouk, Towards the three-dimensional parton structure of the pion: Integrating transverse momentum data into global QCD analysis, Phys. Rev. D **103**, 114014 (2021).

[132] Zhouyou Fan, Huey-Wen Lin, and Matthew Zeilbeck, Nonperturbatively renormalized nucleon gluon momentum fraction in the continuum limit of $N_f = 2 + 1 + 1$ lattice QCD, Phys. Rev. D **107**, 034505 (2023)..

[133] Keh-Fei Liu, Jian Liang, and Yi-Bo Yang, Variance reduction and cluster decomposition, Phys. Rev. D **97**, 034507 (2018).

[134] Yi-Bo Yang, Ming Gong, Jian Liang, Huey-Wen Lin, Keh-Fei Liu, Dimitra Pefkou, and Phiala Shanahan, Nonperturbatively renormalized glue momentum fraction at the physical pion mass from lattice QCD, Phys. Rev. D **98**, 074506 (2018).

[135] Robert G. Edwards and Balint Joo, The Chroma software system for lattice QCD, Nucl. Phys. B, Proc. Suppl. **140**, 832 (2005).